Compressible pressure-based Lattice-Boltzmann applied to humid air with phase change

Isabelle Cheylan, Song Zhao, Pierre Boivin, Pierre Sagaut

Compressible Pressure-Based Lattice-Boltzmann applied to humid air with phase change

Isabelle Cheylan, Song Zhao, Pierre Boivin, Pierre Sagaut

Aix Marseille Univ, CNRS Centrale Marseille, M2P2 UMR 7340, 13451 Marseille cedex 13, France

March 24, 2021

Abstract

A new compressible pressure-based Lattice Boltzmann Method is proposed to simulate humid air flows with phase change. The variable density and compressible effects are fully resolved, effectively lifting the Boussinesq approximation commonly used, e.g. for meteorological flows. Previous studies indicate that the Boussinesq assumption can lead to errors up to 25%, but the model remains common, for compressible models often suffer from a lack of stability. In order to overcome this issue, a new pressure-based solver is proposed, exhibiting excellent stability properties. Mass and momentum conservation equations are solved by a hybrid recursive regularized Lattice-Boltzmann approach, whereas the enthalpy and species conservation equations are solved using a finite volume method. The solver is based on a pressure-based method coupled with a predictor-corrector algorithm, and incorporates a humid equation of state, as well as a specific boundary condition treatment for phase change. In particular, boundary conditions that handle mass leakage are also proposed and validated. Three test cases are investigated in order to validate this new approach: the Rayleigh-Bénard instability applied to humid air, the atmospheric rising of a condensing moist bubble, and finally the evaporation of a thin liquid film in a vertical channel. Results indicate that the proposed pressure-based Lattice-Boltzmann model is stable and accurate on all cases.

1 Introduction

Many application fields require to account for humid air physics when modeling and simulating flows. Examples of important industrial application fields are the simulation of high pressure water vapor flows in steam turbines and the simulation of cooling systems. This is also illustrated by atmospheric flows, in which atmospheric moisture plays a crucial role in the formation of clouds, storms, weather fronts, precipitation and other phenomena [1]. It governs most aspects of our weather and climate in the form of vapor, liquid water, and ice. All these mechanisms can be solved numerically by invoking the Boussinesq approximation [2], which consists in neglecting density variations except in the gravity term in the Navier-Stokes equations. This incompressibility condition simplifies the equations, and is widely adopted in weather forecast tools, but comes with a restriction on the range of flow physics. In fact, it is restricted to small variations of temperature [3], which can be very limiting in the scope of meteorological applications, or

phase change mechanisms. Cherkasov et al. [4] showed that the Boussinesq assumption can lead to an error of 25% in a problem of laminar natural convection in a gas between two vertical isothermal plates heated up to different temperatures, if the temperature of the hot wall is no more than three times the temperature of the cold wall. Schatzmann [5] also studied a variety of industrial stack plumes with different initial density ratios, and made comparisons of predictions with and without the Boussinesq approximation. It was found that the difference in jet-property predictions between the two models increases with increasing initial density defect ratio. In the case of the largest ratio tested, the maximum height of rise predicted with the Boussinesq model was 20% larger than with the non-Boussinesq model. This shows the importance of a non-Boussinesq model to study cases with large differences of temperature, or more generally cases where the thermodynamic variables vary a lot. Other less restrictive assumptions, such as using pseudo-incompressible equations [6], or anelastic equations [7], can also be used, which all rely on simplifications of the fully compressible Navier-Stokes equations to tackle the compressibility issue. Previous studies have also demonstrated that it is possible to use a full compressible model: Feng and Tao [8] developed a full compressible thermal model using a multispeed lattice Boltzmann method, but the cost of this method is prohibitive for an industrial use as will be explained in section 3.2. Another solution to reduce the cost of a compressible solver is to couple a finite volume method to a Lattice-Boltzmann model as was shown by Luan et al [9]. They applied their model to a case of natural convection and obtained stable results, but their study was restricted to single component flows. The main disadvantage of the compressible model is its lack of stability as shown by Guiho [10]. This stability issue of the compressible model will also be demonstrated with the third test case presented here, because a stable solution with the density-based solver could not be obtained. In order to overcome this problem, the objective of our study is to broaden the scope of application of the compressible model thanks to an improved solver stability. The novelty of our method is to propose a stable multi component compressible solver that can handle humid air for meteorological applications, and to achieve a better accuracy without using the common Boussinesq assumption. New boundary conditions will also be proposed in order to handle the mass leakage at boundaries. The rest of the introduction will focus on the features of our pressure-based compressible hybrid Lattice-Boltzmann method.

Most previous studies dealing with humid air and moist cases are based on the Navier-Stokes equations, e.g. [11, 12, 13]. Here, we chose to use the Lattice-Boltzmann method (LBM) which is a mesoscopic approach, based on the Boltzmann equation, that recovers the Navier-Stokes equations on the macroscopic level. The advantages of the LBM are its automatically generated cubic mesh which removes the need of a body-fitted mesh, as well as its very high parallel efficiency and very high numerical accuracy. The LBM has been gaining more and more interest in the industry, with practical applications in the automotive industry, the aerospace industry, but also in civil engineering, among other applications. Feng et al. [14] have also developed the LBM for meteorological applications, and their study will serve as a guideline for this article. Nevertheless, they use the Boussinesq approximation which is not the case here as explained previously.

The novelty of the present work is that a new fully compressible pressure-based Lattice-Boltzmann solver with a hybrid recursive regularization is used and developed in order to incorporate specific features: the humid air equation of state, the phase

change mechanisms and the evaporation/condensation boundary conditions. Because of the presence of a small fraction of liquid in the humid air, the perfect gas law cannot be used. Instead, a humid air equation of state is used, e.g. see [1, 15]. This equation of state, which originates in a linearization of a full multispecies multiphase equation of state makes it possible to study cases with small fractions of water vapor and liquid. Phase change between the vapor and the liquid is also taken into account and evaporation/condensation processes can therefore be simulated. In order to do so, the instantaneous equilibrium phase change model given in [15] is used to simulate the condensation of a bubble rising in a moist atmosphere, but also the evaporation of a thin liquid film at the walls of a heated channel [16]. Special attention is thus given in order to incorporate the phase change mechanisms in the boundary conditions. In order to account for phase change mechanisms, an enthalpy equation is used in the present work instead of the entropy equation used in [17]. This hybrid method is based on the coupling of the mass and momentum equations solved by the LBM, with the enthalpy equation solved by a finite-difference method. Doing so, one does not need (when simulating fully compressible flows) to expand the equilibrium function up to an order too expensive for an industrial use. The regular D3Q19 lattice can thus be kept, and the general cost of the solver, which is fully compressible, stays reasonable.

Another aspect of the solution is the HRR collision model, which damps non-physical modes which can lead to instabilities at high Reynolds number flows. The HRR collision model stabilizes the solution and makes it possible to use the solver in a more general framework [18, 19]. The last novel aspect of this LBM algorithm is the development of a new segregated, pressure-based approach, coupled with a predictor-corrector method [17]. The predictor-corrector method is an algorithm in which the first step (predictor) consists in finding the weakly compressible solution. Then, the second step (corrector) is to correct the first step in order to recover a fully compressible solution. This type of algorithm is quite common in Navier-Stokes methods, and its efficiency depends on the robustness and capability of the first step. Here, only explicit schemes are used for both steps and the predictor step is based on the artificial compressibility method pioneered by Chorin [20]. The pressure-based collision model is used for the first step (predictor) of the algorithm. Pressure-based methods present an advantage in some cases which is the following: by controlling explicitly the pressure oscillations in flows with a large density variation, pressure-based solvers have proven to be more robust and accurate than classical single relaxation time density-based LBM solvers. Indeed, computing the pressure directly from an evolution equation, and not from the equation of state, reduces spurious pressure oscillations in multifluid Navier–Stokes methods, see[21, 22] and in Lattice-Boltzmann Methods [23, 24, 25]. Nevertheless, the predictor step gives a pressure evolution equation which is not valid for high-Mach number flows, hence the need for a correction step to recover the full compressible solution.

This article is organized as follows: the first section presents the governing equations of the method, beginning with the macroscopic equations and the specific features needed for the humid air applications : the humid equation of state, the phase change mechanisms, and the special boundary conditions for evaporation/condensation. The numerical method is then presented, with the pressure-based LBM coupled with a predictor-corrector algorithm and the finite volume method to solve the species and the enthalpy conservation equations. In the second section, the test cases are presented in

increasing order of complexity. First, the Rayleigh-Benard instability is studied, in a single component configuration (dry air), and then in a multiple components configuration (dry air with water vapor and water liquid). This first test case will prove that the pressure-based code gives consistent results in a simple configuration, and is compared to the density-based code. The second test case deals with a moist bubble rising in the atmosphere, which is condensing during its rise. The purpose of this second test case is to demonstrate that the full compressible effects are taken into account in a large domain, without using the Boussinesq assumption, which is most commonly used in the meteorological context as shown by previous studies [26, 27]. Finally, the last test case is about a heated vertical channel with a thin liquid film on its walls. Dry air is entering the channel from the top, and produces the evaporation of the thin liquid film, thus creating vapor at the wall. This last case shows the superiority of our model compared to the density-based code, because the latter did not give usable results contrary to the former. All the test cases are performed with the pressure-based version and compared to the density-based version of the code when possible, and/or to the reference when available, in order to validate the accuracy and robustness of the pressure-based method.

2 Governing equations

2.1 Macroscopic equations

The humid air flow is assumed to follow the compressible Navier-Stokes equations, linking the local mass volume ρ, velocity vector u_α and energy.

Under this formalism, mass and momentum conservation read

$$\frac{\partial \rho}{\partial t} + \frac{\partial \rho u_\beta}{\partial x_\beta} = 0 \tag{1}$$

$$\frac{\partial \rho u_\alpha}{\partial t} + \frac{\partial \rho u_\alpha u_\beta + \delta_{\alpha\beta} p - \Pi_{\alpha\beta}}{\partial x_\beta} - \rho g = 0, \tag{2}$$

where p is the pressure, to be linked to the local state in Eq. (7), g is the gravity acceleration, and $\Pi_{\alpha\beta}$ is the stress tensor

$$\Pi_{\alpha\beta} = \mu \left(\frac{\partial u_\alpha}{\partial x_\beta} + \frac{\partial u_\beta}{\partial x_\alpha} - \delta_{\alpha\beta} \frac{2}{3} \frac{\partial u_\gamma}{\partial x_\gamma} \right). \tag{3}$$

Energy conservation is considered in its enthalpy h form,

$$\frac{\partial h}{\partial t} + u_\alpha \frac{\partial h}{\partial x_\alpha} = \frac{1}{\rho} (\Pi_{\alpha\beta} \frac{\partial u_\alpha}{\partial x_\beta} - \frac{\partial q_\alpha}{\partial x_\alpha} + \frac{Dp}{Dt}), \tag{4}$$

where the pressure derivative $\frac{Dp}{Dt}$ is assumed to be negligible, and q_α is the heat flux, assumed to depend on the temperature T as

$$q_\alpha = -\lambda \frac{\partial T}{\partial x_\alpha} + \rho \sum_k^N h_k Y_k V_{k,\alpha}, \tag{5}$$

with λ the thermal conductivity. It is defined as:

$$\lambda = \frac{\mu}{Pr} \sum_k Y_k C_{p,k} \tag{6}$$

$V_{k,\alpha}$ is the diffusion velocity and it is evaluated through a Fickian approximation.

2.2 Moist equation of state and phase change

To close the system of governing equations, a thermodynamic closure is required, linking the pressure with the mass volume and energy (or enthalpy / temperature). Considering a mixture of dry air, water vapor, and liquid water with respective mass fractions Y_d, Y_v and Y_l, and assuming that mass fractions of vapor and liquid water remain small, one obtains the following equation of state [1, 15],

$$\rho r T = p(1 - 0.61 Y_v)(1 + Y_l), \tag{7}$$

where r is the mass gas constant of dry air.

The enthalpy h is linked to the temperature T through

$$h = \sum_{k=1}^{3} h_k Y_k, \tag{8}$$

with

$$h_k = C_{p,k} T + q_k. \tag{9}$$

$C_{p,k}$ is the constant pressure mass heat capacity of species k, and q_k its reference enthalpy. The mean heat capacity C_p therefore reads

$$C_p = \sum_k Y_k C_{p,k} \tag{10}$$

For the rest of the demonstration, we introduce the following thermodynamic quantity:

$$\theta = \frac{p}{\rho c_s^2} = \frac{rT}{c_s^2} \tag{11}$$

as the ratio of thermodynamic perfect gas pressure to the classical athermal LBM pressure.

In considering three constituents, two additional conservation equations need to be appended to the system as

$$\frac{\partial Y_v}{\partial t} + u_\alpha \frac{\partial Y_v}{\partial x_\alpha} = \frac{1}{\rho} \frac{\partial}{\partial x_\alpha} (\rho D_y \frac{\partial Y_v}{\partial x_\alpha}) - \dot{Q} \tag{12}$$

$$\frac{\partial Y_l}{\partial t} + u_\alpha \frac{\partial Y_l}{\partial x_\alpha} = \frac{1}{\rho} \frac{\partial}{\partial x_\alpha} (\rho D_y \frac{\partial Y_l}{\partial x_\alpha}) + \dot{Q}, \tag{13}$$

where D_y is the diffusion coefficient, given by the Schmidt number of each specie:

$$D_y = \frac{\mu}{\rho S c_y} \tag{14}$$

and $\dot{Q}$ is a source term, accounting for potential phase change. The dry air mass fraction is deduced as $Y_d = 1 - Y_v - Y_l$.

Phase change, i.e. condensation or evaporation, is formulated as in the NCAR general atmospheric model [28]: condensation takes place when saturation is reached at a given grid point, and the specific humidity is bounded by the saturation value Y_v^{sat}:

$$Y_v^{sat} = \frac{\epsilon p_{sat}}{p - (1 - \epsilon p_{sat})}, \tag{15}$$

where $\epsilon = 0.622$ is the ratio of molecular masses of water vapor and air. The saturation pressure is assumed to follow an Antoine law

$$p_{sat}(T) = 610.78 e^{(17.269 \frac{T-273.16}{T-35.86})}. \tag{16}$$

The phase change source term is then computed through a saturation adjustment [15]:

$$\dot{Q} = \begin{cases} -Y_l/\delta_t & \text{if} \quad Y_v < Y_v^{sat} \quad \text{and} \quad Y_l < \Delta Y_v \\ \Delta Y_v/\delta_t & \text{otherwise} \end{cases} \tag{17}$$

where

$$\Delta Y_v = \frac{C_p r T^2}{\epsilon Y_v^{sat} L_v(T)^2 + C_p r T^2} (Y_v - Y_v^{sat}), \tag{18}$$

with the mass latent heat L_v defined as

$$L_v(T) = h_v(T) - h_l(T). \tag{19}$$

3 Numerical method

We now present the hybrid numerical method used to solve the governing equations. Mass and momentum conservation equations (1) and (2) are solved via a pressure-based Lattice-Boltzmann solver, coupled with a finite volume solver for energy and species equations (4), (12) and (13). The novelty of the method relies on the fact that the full compressible effects are taken into account, contrary to previous studies on the matter which use the Boussinesq assumption as explained in the introduction. Another novel aspect of our approach is the mass conserving boundary conditions, which have been developed specifically to handle mass leakage at the boundaries when the simulation domain is big, which is typical of meteorological applications.

3.1 Pressure-based Lattice-Boltzmann solver coupled to a predictor-corrector approach

Lattice-Boltzmann methods rely on a discretization on space, time, and velocity of the Boltzmann equation [29, 30]. f_i represents the variable solved by the LBM, and corresponds to the density distribution of particles at space and time (x, t) with velocity c_i. It is a mesoscopic approach which recovers the macroscopic quantities through the moments of the distribution function f_i:

$$\begin{cases} \sum_i f_i^{eq} = \rho\theta = p/c_s^2 \\ \sum_i c_{i,\alpha} f_i^{eq} = \rho u_\alpha \\ \sum_i c_{i,\alpha} c_{i,\beta} f_i^{eq} = \rho u_\alpha u_\beta + \rho\theta c_s^2 \delta_{\alpha\beta} \end{cases} \tag{20}$$

The Lattice-Boltzmann equation, discretized in space, time, and velocities, is written:

$$f_i(x + c_i\delta_t, t + \delta_t) = f_i^{eq}(x, t) + (1 - \frac{1}{\tau}) f_i^{neq}(x, t) + \frac{1}{2} F_i^E(x, t) \tag{21}$$

The term $F_i^E(x,t)$ accounts for the gravity term F_i^g and for correction terms [17]. There are several ways to include an external force into the LBM. Here, we use the approach from [31] in which the gravity term is written as follows:

$$F_i^g = \rho\omega_i[\frac{A_\alpha c_{i\alpha}}{c_s^2} + \frac{(u_\alpha A_\beta + u_\beta A_\alpha)(c_{i\alpha}c_{i\beta} - c_s^2\delta_{\alpha\beta})}{2c_s^4}] \tag{22}$$

In this approach, when an external force is taken into account, such as gravity, the macroscopic velocity is also modified as:

$$u = \frac{1}{\rho}\sum_i c_{i,\alpha} f_i^{eq} + \frac{A}{2} \tag{23}$$

The other correction terms included in F_i^E are detailed in Farag et al [17].

The equilibrium function is written:

$$f_i^{eq} = \omega_i[\rho\theta + \frac{c_{i\alpha}\rho u_\alpha}{c_s^2} + \frac{a_{\alpha\beta}^{(2),eq} H_{i\alpha\beta}^{(2)}}{2c_s^4} + \frac{a_{\alpha\beta\gamma}^{(3),eq} H_{i\alpha\beta\gamma}^{(3)}}{6c_s^6}] \tag{24}$$

where $H_{i\alpha\beta}$ and $H_{i\alpha\beta\gamma}$ are respectively the second and third order Hermite polynomials. The non equilibrium distribution function is also expanded in Hermite polynomials and reconstructed by a Recursive Regularized BGK LBM [18, 19] :

$$f_i^{neq} = \omega_i[\frac{a_{\alpha\beta}^{(2),neq} H_{i\alpha\beta}^{(2)}}{2c_s^4} + \frac{a_{\alpha\beta\gamma}^{(3),neq} H_{i\alpha\beta\gamma}^{(3)}}{6c_s^6}] \tag{25}$$

In the present approach, the non-equilibrium coefficients $a_{\alpha\beta}^{(2),neq}$ and $a_{\alpha\beta\gamma}^{(3),neq}$ are evaluated with the hybrid recursive collision model introduced in [18]. This model is used to enhance numerical stability, as well as enforce a traceless lattice-Boltzmann tensor by removing its trace. It is observed to yield accurate and robust results for a broad range of applications and flow physics, e.g. [32, 33, 14, 34, 35].

The pressure-based solver is very similar to the density-based solver, except that the macroscopic equations which are recovered are a slightly different due to the change in the zeroth order moment $\rho\theta$. In the pressure-based solver, the macroscopic equation on mass which is recovered is the following:

$$\frac{\partial\rho\theta}{\partial t} + \frac{\partial\rho u_\beta}{\partial x_\beta} = 0 \tag{26}$$

This equation represents the pressure evolution equation in the low-Mach nearly incompressible limit, but it is not valid in fully compressible flows with strong dilatational effects. A few corrections are necessary in order to recover the full compressible limit (which correspond to the corrector step mentioned above). The corrections, done on the zeroth order moment and on the second order moment, are the following:

$$\rho(t+\delta t, x) = \sum_i f_i^*(t+\delta t, x) + \rho(t,x)[1-\theta(t,x)] \tag{27}$$

$$a_{\alpha\beta}^{cor} = c_s^2\delta_{\alpha\beta}[\rho(t+\delta t,x)(1-\theta(t+\delta t,x)) - \rho(t,x)(1-\theta(t,x))] \tag{28}$$

More details about the pressure-based LBM algorithm and on the correction terms can be found in Farag et al. [17].

3.2 Finite volume solver for species and enthalpy

A first-order explicit Euler scheme is used for the time integration :

$$\phi^{n+1} = \phi^n + \delta_t[RHS_C(\phi^n) + RHS_D(\phi^n) + \Phi] \tag{29}$$

where RHS_C, RHS_D represent the convection term and the diffusion term, respectively. The convective flux is constructed using the MUSCL scheme [36], with the van Albada limiter [37]. A classical second order central difference scheme is adopted for the diffusion term. The last term Φ is related to remaining source terms, which are treated explicitly in time.
It is also possible to solve the scalar transport and the enthalpy equations by using the LBM, with the multiple distribution function model for example [38], or a multispeed approach [8]. Nevertheless, these methods are more cumbersome numerically than the hybrid method proposed here as noted by [39], which is why we decide to couple the LBM with a finite volume solver for the species and enthalpy equations.

3.3 Boundary conditions

In the LBM, several types of boundary conditions can be used, which can be classified mainly in two types : the conditions which deal with distribution functions directly (such as Bounce-Back and interpolated Bounce Back conditions [40, 41]), and the conditions which deal with macroscopic quantities from which distribution functions are then deduced, or reconstructed, hence the term "reconstruction" method [42, 43] for this second approach. The reconstruction method can be summarized with the following steps:

- Depending on the desired boundary condition, we apply the Dirichlet or Neumann condition to macroscopic quantities : velocity, density, enthalpy, and species
- Reconstruction of f_i^{eq} from macroscopic values on boundaries (eq 24)
- Reconstruction of f_i^{neq} from macroscopic values on boundaries (eq 25)
- Computation of f_i using f_i^{eq} and f_i^{neq}

Details of the present implementation are available in [44, 45, 46] and will not be repeated here for the sake of brevity.

For enthalpy and species which are solved via the finite volume approach, the macroscopic values of h, Y_l, Y_v are simply imposed (Dirichlet condition) or extrapolated (Neumann condition) on all boundaries via a first order interpolation.

This approach is most commonly used in industrial applications, because it is possible to use some already existing conditions (wall models for turbulent applications for example) which have been developed on macroscopic quantities, often for Navier-Stokes solvers. On the other hand, the mass conservation on solid impermeable boundaries is not necessarily respected in the reconstruction method. For many types of engineering problems for which the numerical domain is small and gravity does not play a big role, it is not an important concern. Nevertheless, the mass conservation issue with the reconstruction method can cause a problem for cases in which gravity plays an important role

because the numerical domain is large (atmospheric test cases for example). In that case, the leakage of mass at the boundaries can lead to inaccuracy and stability issues. This type of problem was encountered here for the bubble ascending in a moist atmosphere case. It was therefore mandatory to respect the mass conservation at the boundaries. To do so, it is easier to use the first approach: handling distribution functions directly. For compressible problems, respecting the mass conservation at the boundary can be mathematically written:

$$\frac{dm}{dt} = \int_V \frac{d\rho}{dt} dV = -\int_V \nabla(\rho u) dV = -\int_S \rho u_n dS = 0 \tag{30}$$

with n the normal vector of the boundary S. Knowing that in the LBM, $\rho u_n = \sum_i c_i f_i$, this leads to a condition on the functions coming out and coming in the domain at the boundary, which resembles the bounce-back method.

$$\sum_{\text{outgoing } i} c_i f_i(x_k, t_n) + \sum_{\text{incoming } i} c_i f_i(x_k, t_n) = 0 \tag{31}$$

If we use the bounce back condition for the incoming unknown direction:

$$\sum_{\text{outgoing } i} c_i f_i^{col}(x_{k-1}, t_{n-1}) + \sum_{\text{incoming } i} c_i f_i^{col}(x_k, t_n) = 0 \tag{32}$$

If we suppose that the boundary is flat (which is the case in the bubble test case), and knowing that $c_i = -c_{opp(i)}$ with $opp(i)$ the opposite direction of i, the condition is written:

$$f_i^{col}(x_k, t_n) = f_{opp(i)}^{col}(x_{k-1}, t_{n-1}) \tag{33}$$

with i the incoming direction.

4 Validation of the method

The proposed new pressure-based fully compressible Lattice Boltzmann Method for humid air will now be validated considering several test cases.

4.1 Rayleigh-Bénard instability

The Rayleigh-Benard instability is a natural convection phenomenon, in which a fluid is enclosed between two horizontal plates, the one below being heated and the one on top being cooled, so that the fluid develops a regular pattern of convection cells known as Benard cells. It is an important mechanism of mass and heat transfer in nature (meteorology, astrophysics) and in many industrial applications (heat exchangers). The gravity accelerates the flow downwards whereas the viscosity counteracts the motion so that a convection pattern appears. The Prandtl number Pr and Rayleigh number Ra are defined as:

$$Pr = \frac{\nu}{D} \tag{34}$$

$$Ra = Pr \frac{gH^3 \Delta T}{\nu^2 T_0} \tag{35}$$

ΔT is the temperature difference between the top and bottom walls, T_0 is the reference temperature set to 300.0 K, H is the domain height set to 1m, and ν is the kinematic viscosity given by the value of Ra in the simulations. For the test cases presented in this section, the Rayleigh number is equal to 10^4 and the Prandlt number is equal to 0.71. Another important parameter is the reference velocity used to scale the velocity on figure 3:

$$u_0 = \sqrt{g\beta H \Delta T} \tag{36}$$

4.1.1 Single component case : dry air

This test case is studied in a square domain, the top wall being cooled at $T_C = 299.5$ K and the bottom wall being heated at $T_H = 300.5$ K. Adiabatic conditions are set for the temperature on the right and left walls. The temperature difference $T_H - T_C$ is chosen to be small enough to allow the comparison with results based on the Boussinesq approximation.

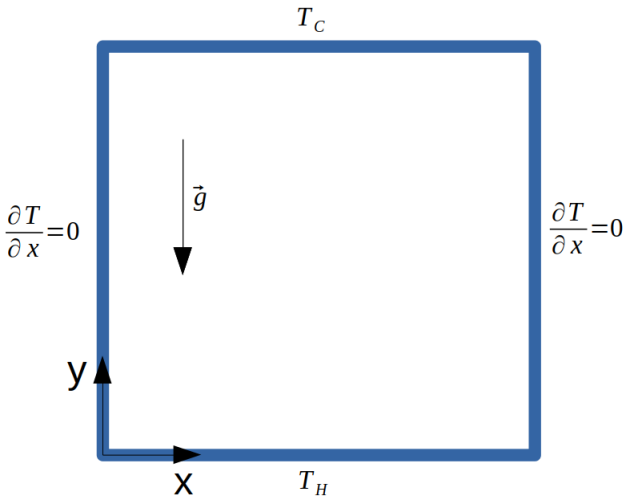

Figure 1: *Schematic diagram of the single component Rayleigh-Benard case*

Only dry air is simulated in this first test case, so that the pressure-based code can be validated and compared to results from Feng et al. [14], and Ouertatani et al [47] in which a nearly incompressible model was used along with a Boussinesq approximation. The square simulation domain is $1m \times 1m$, on a 50×50 grid. Figure 2 shows the temperature field once the steady state has been reached. It is in good agreement with reference [14].

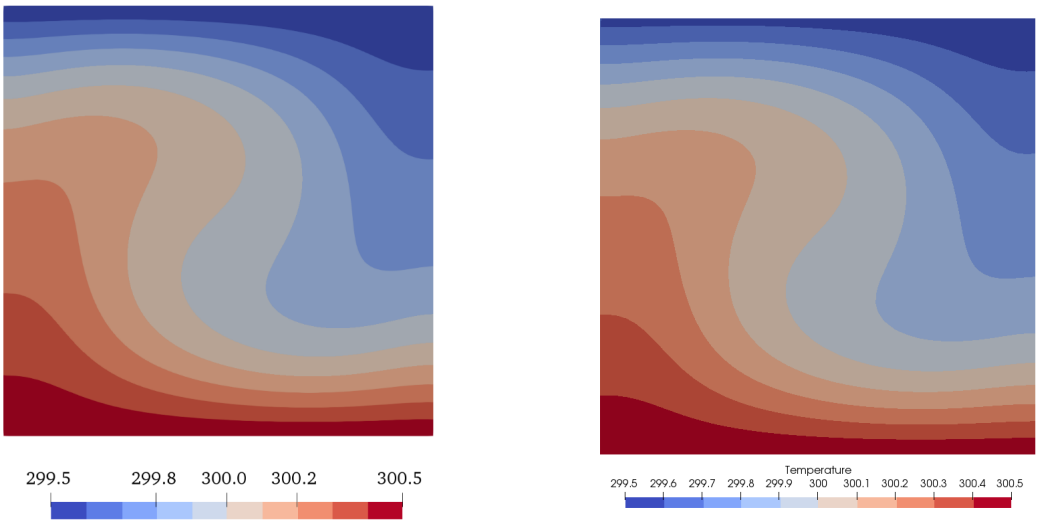

Figure 2: *Temperature for the single component case : reference [14] (left) and pressure-based solver (right)*

The comparisons of the vertical velocity u_y along a horizontal line in the middle of the domain, and of the horizontal velocity u_x along a vertical line in the middle of the domain, are presented on figure 3.

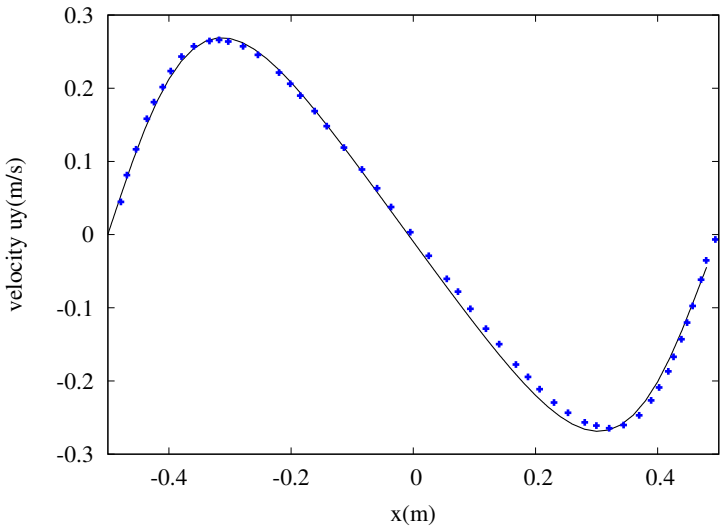

Figure 3: *Velocity u_y along x at midline of domain for the single component case. Symbol = reference, line = pressure-based solver*

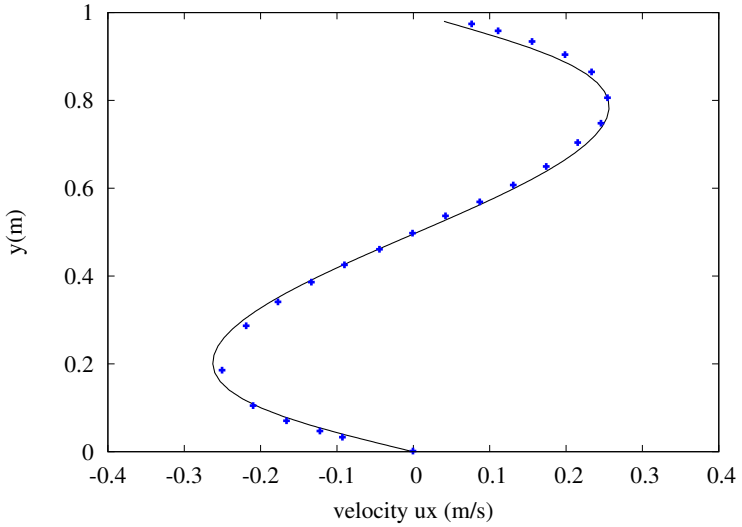

Figure 4: *Velocity u_x along y at midline of domain for the single component case. Symbol = reference, line = pressure-based solver*

The results are in very satisfactory agreement with the reference data, meaning that the pressure-based LBM solver can be accurately used to investigate flows in the Boussinesq regime. The slight differences observed may be due to the fact that our pressure-based solver does not rely on the Boussinesq assumption, contrary to the references [14, 47]. Indeed, we can assume that without the Boussinesq assumption, in the momentum and mass equations, the density variations (others than in the buoyancy force) are not neglected, hence leading to small differences between the reference and the results presented here.

4.1.2 Multiple component case : moist air (dry air with water vapor and water liquid)

This test case presents a multiple component Rayleigh-Bénard instability, which is composed of dry air, water vapor, and water liquid. The water vapor and liquid fractions are set respectively to 0.002 and 0.001 on the top wall, and to 0 on the bottom wall. The bottom wall is heated at 309.5K and the top wall is cooled at 299.5K. Periodic boundary conditions are applied at the left and right walls. The domain is extended to observe several convection cells. The temperature field is displayed on figure 5. Because the reference article does not present results with the gravity applied to all three components, but only to water components, the comparison is made between the density-based version of the ProLB solver, and the present pressure-based version. Indeed, the density-based version of ProLB has already been validated in many cases [35, 44] and will serve as a reference guideline when no data is available in the literature.

Figure 5 presents the temperature field: several convection cells can be observed in the extended domain.

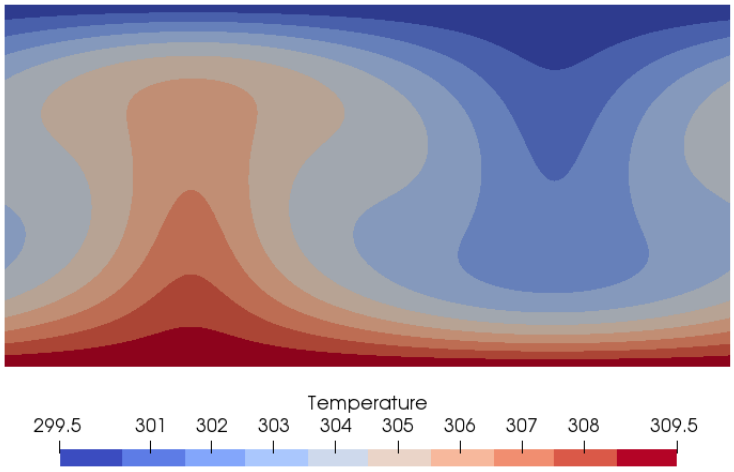

Figure 5: *Temperature for the three component Rayleigh-Benard case*

A comparison of the density and velocity fields predicted using the pressure-based and density-based methods is then made. The comparison is done on a horizontal and a vertical lines in the middle of the domain on Figs. 6 and 7, respectively.

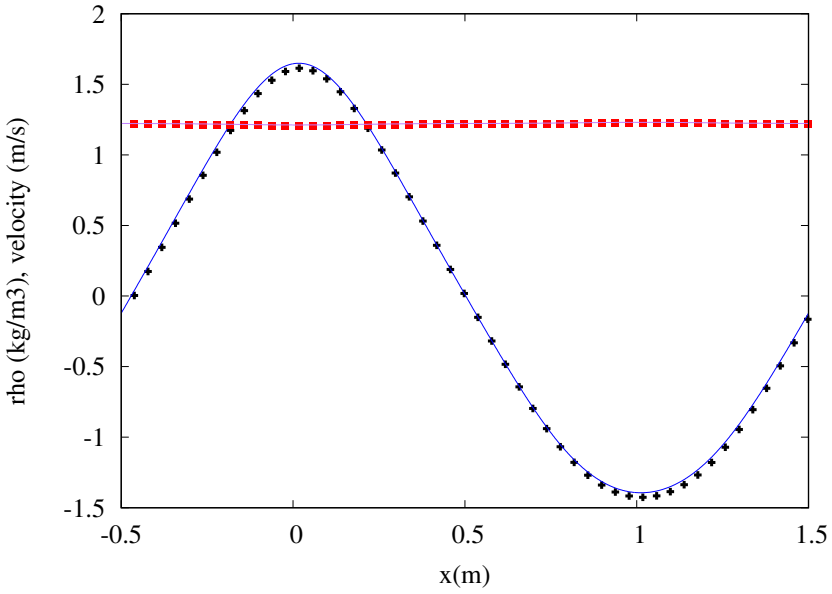

Figure 6: *Velocity (cross) and density (square) on a horizontal line at the middle of the domain. Symbols = reference data (density-based method), solid line = pressure-based solver*

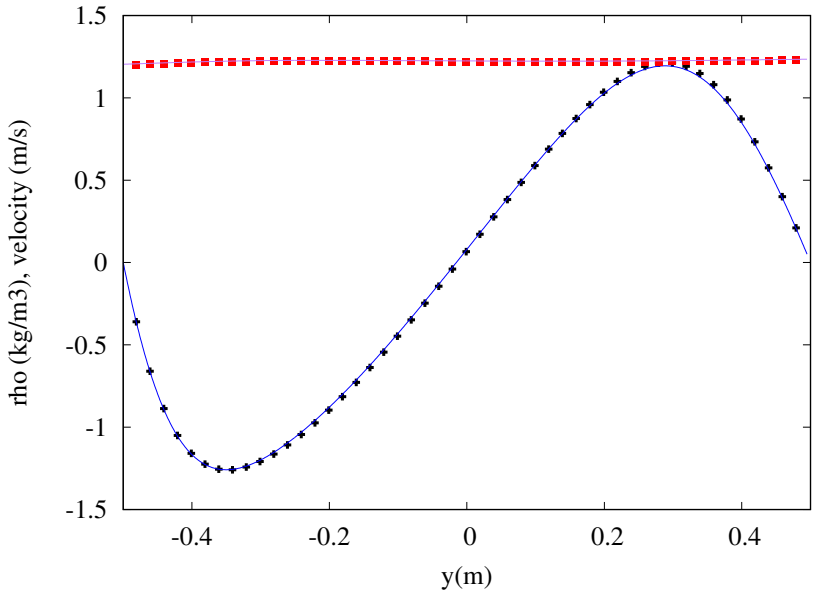

Figure 7: *Velocity (cross) and density (square) on a vertical line at the middle of the domain. Symbols = reference data, solid line = pressure-based solver*

A very good agreement is obtained between the density-based and pressure-based methods, which means that the new pressure-based code can be accurately used to simulate moist convection cases, with several components. Here, both density-based and pressure-based codes give good results and demonstrate good accuracy and robustness.

4.2 Rising bubble

A rising moist bubble is studied in a two dimensional domain, with a height of 2.4 km and a width of 3.6 km, on a 720 x 480 grid with a 5m mesh size. The base state has a constant relative humidity of 20% with a pressure of 850 hPa and a surface temperature of 283 K. The bubble is initially located at the center of the domain, at z = 0.8 km. The kinematic viscosity ν is set to 1 m^2/s and the Prandlt number to 1. The relative humidity RH is set to 100% inside the bubble, for $r < 200m$. A transition layer is assumed for $200m < r < 300m$, defined as follows :

$$RH = 20\% + 80\%\cos^2(\frac{\pi}{2}\frac{r-200}{100}) \tag{37}$$

The vapor mass fraction can then be deduced as:

$$Y_v = \frac{\epsilon.p_{sat}RH}{p_0 - RH(1-\epsilon)p_{sat}} \tag{38}$$

Concerning other initial conditions, we cannot use the reference initial conditions from [48, 14], which were based on a nearly incompressible approach. Indeed, in these references a constant density ρ_0 is used as a reference state. This is possible when invoking the Boussinesq approximation, because density variations are only taken into account in the gravity term via a modified and special formulation of the gravity. Here, we use a fully compressible solver, which means that setting a constant initial density is not correct nor representative of the hydrostatic atmospheric state. The correct way

to initialize the simulation is to find the initial state (p, ρ, T) which respects the perfect gas law, the hydro static equilibrium state, and another constraint on the temperature. Several assumptions on the atmospheric temperature field can be made: isothermal atmosphere, or linear variation of the temperature for example. Here, we chose to use the latest, which leads to the following set of equations:

$$\begin{cases} p = \rho RT \\ \frac{dp}{dz} = -\rho g \\ \frac{dT}{dz} = -K \end{cases} \tag{39}$$

Solving the previous system of equations leads to the following expression of the initial state:

$$\begin{cases} p = p_0(1 - \frac{Kz}{T_0})^{(g/RK)} \\ \rho = \frac{P}{RT} \\ T = T_0 - Kz \end{cases} \tag{40}$$

The coefficient K is set to 0.0065 here, so that the temperature varies linearly from 283 K (ground surface) to 267.4 K (top surface).

Regarding boundary conditions, both boundary conditions explained in section 3.3 were tested on a simplified 2.4km high air column with identical initial conditions as the bubble test case. Because the fluid is initialized to the hydrostatic state, there should be no movement of fluid in the air column and the velocity should be equal to zero. When using the reconstruction method, we encountered mass conservation issues at the boundaries due to the presence of gravity in a very high domain. Nonphysical mass flux is coming in the domain because the top and bottom walls do not conserve exactly the mass with the reconstruction method. To solve this problem, we used the second boundary condition (33) explained in section 3.3 which conserves the mass. The result with both boundary conditions is displayed on Fig. 8 :

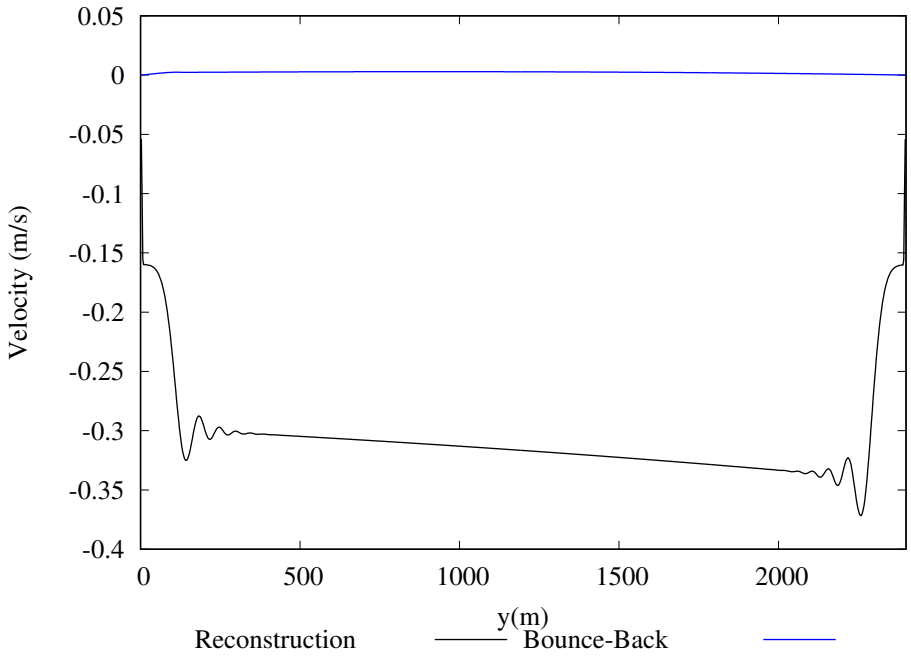

Figure 8: *Vertical velocity in the air column for two types of boundary condition implementations*

The mass coming in the domain with the BB boundary condition is better controlled with incoming velocity values of the order of $1e^{-3}m/s$ compared to $1e^{-1}m/s$ with the reconstruction method. We will hence use the bounce back condition for the bubble test case.

The contour of water vapor is displayed on figure 9.

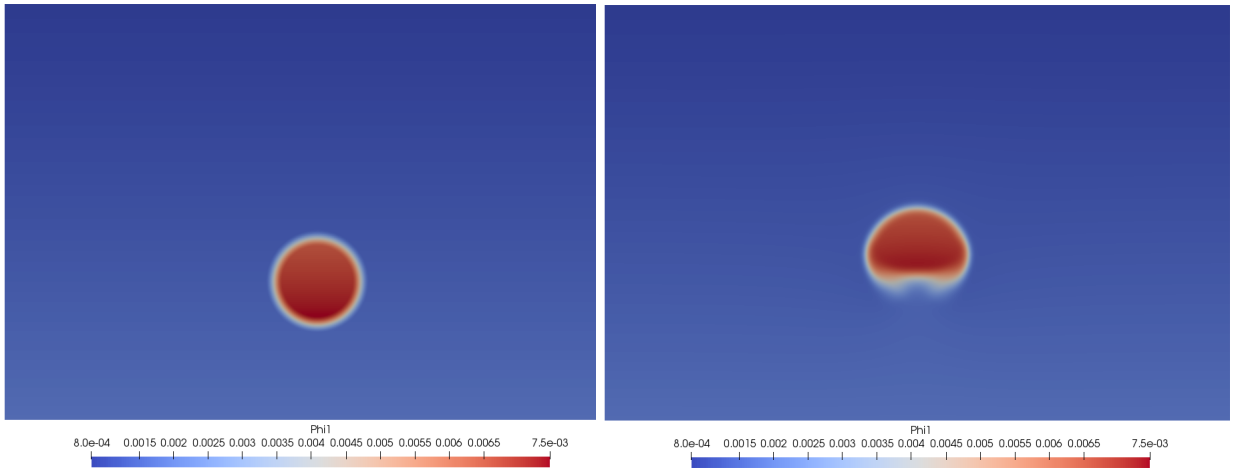

Figure 9: *Vapor contour at initial time (left) and at $t = 150s$ (right)*

The bubble rises and expands over time, condensing during its rise as predicted by the reference. Nevertheless, a quantitative comparison with the reference article is not possible because the initial states are different, as it is not possible to impose a

constant reference density initially since the Boussinesq assumption is not used here. In order to illustrate this problem, figure 10 shows a comparison of the initial densiy and temperature, in the Boussinesq reference case and in our pressure-based compressible solver. Imposing a constant density field initially led to a non physical result in our case, because we do not use the Boussinesq assumption due to the compressible formulation of our solver, so it was mandatory to impose a varying density initially, which agrees with the hydrostatic solution. Because of this initial difference, the results quickly differ: at two minutes, the highest position of the bubble in our case is 1152m, 5% above the measured position 1100m in the reference. At three minutes, the order of error is 10%, the bubble being located at 1352m in our case, against 1194m in the reference.

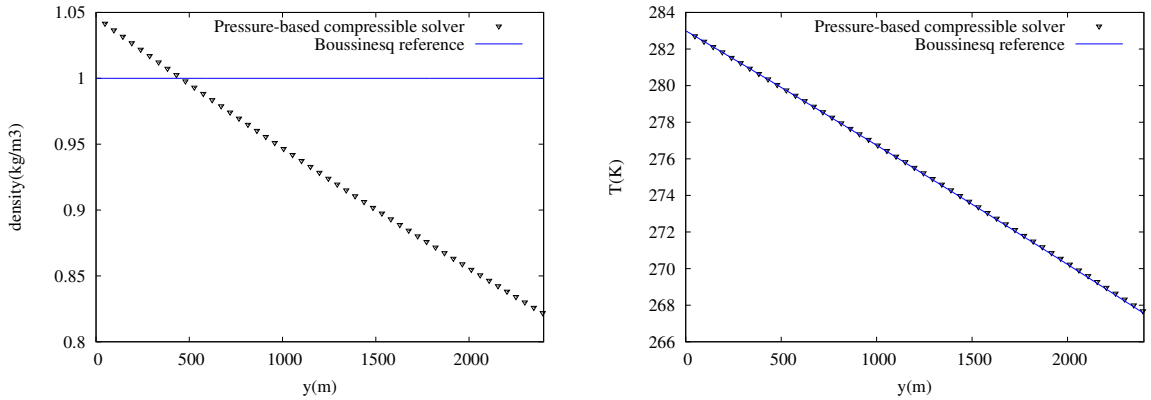

Figure 10: *Initial condition for the density (left) and for the temperature (right)*

In the same manner as in the first test case, a comparison between the density-based and pressure-based codes is done, based on the fact that the density-based code has been validated on numerous cases. The profiles of density, temperature, vapor mass fraction and velocity are compared on Figs. 11, 12, 13 and 15.

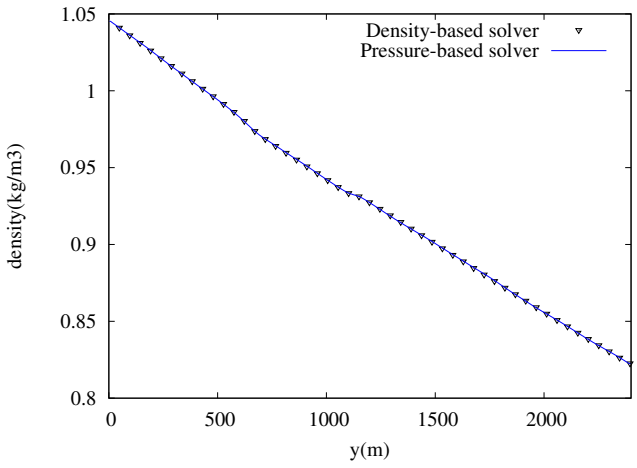

Figure 11: *Profiles of density along a vertical line x=1800m at t=100s*

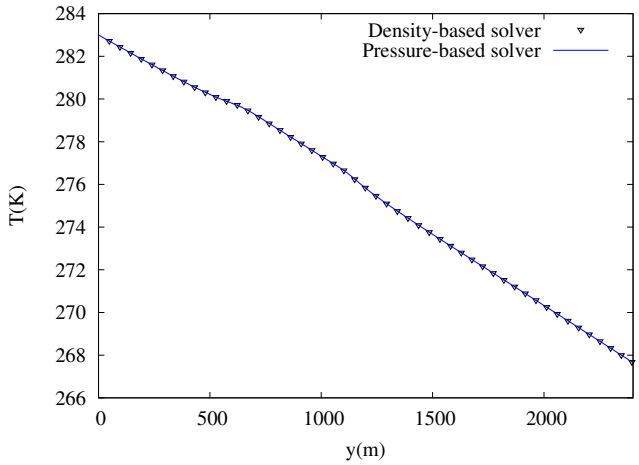

Figure 12: *Profiles of temperature along a vertical line x=1800m at t=100s*

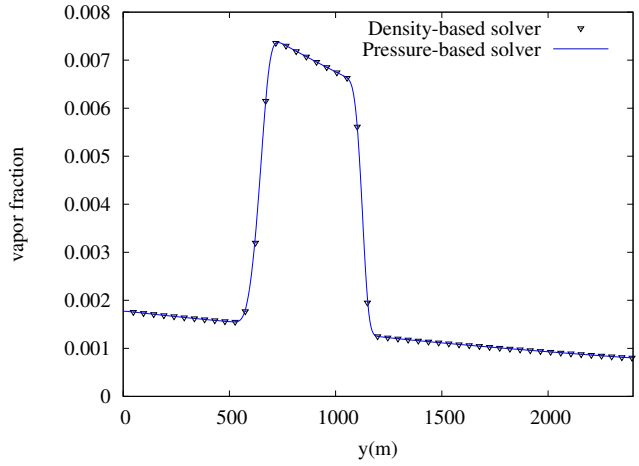

Figure 13: *Profiles of vapor fraction along a vertical line x=1800m at t=100s*

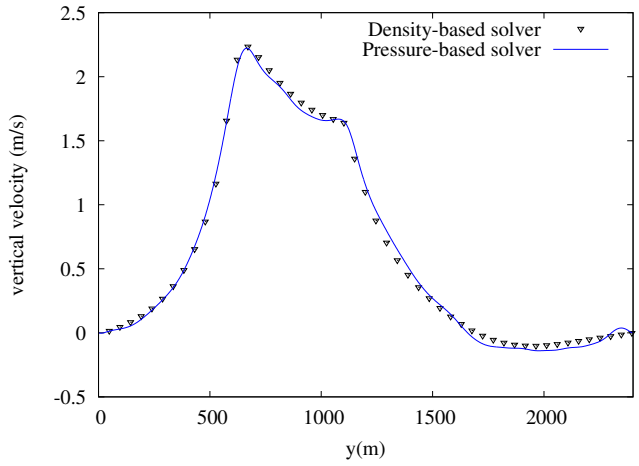

Figure 14: *Profiles of vertical velocity along a vertical line x=1800m at t=100s*

Both density-based and pressure-based codes give almost identical profiles. The results are in good agreement with [48], with the bubble expanding and condensing during its rise.

4.3 Heated vertical channel with evaporating liquid film

The last test case deals with a heated vertical channel with evaporating thin liquid films at the walls in which a steady, downward, laminar flow is streaming. This test case shows that the pressure-based LBM solver also includes condensation/evaporation boundary conditions, which are stable and accurate. In order to validate the results, a reference case from [16] is selected. First, it is assumed that the liquid films are extremely thin so that the boundary conditions for heat and mass transfer from [49] can be used. At the inlet section, the fluid temperature, velocity, and vapor mass fraction are constant and uniform, and the pressure is interpolated. At the outlet section, the pressure is constant and equal to the atmospheric pressure, and the fluid velocity, temperature and vapor mass fraction are interpolated. At the walls, we assume that the gas and liquid film interface are in thermodynamic equilibrium, which leads to the following expression for the vapor mass fraction at the wall under the extremely thin liquid film assumption:

$$Y_{v,w} = \frac{M_v}{M_a} \frac{p_{sat}(T_w)}{p - p_{sat}(T_w)(1 - \frac{M_v}{M_a})} \tag{41}$$

Liquid evaporation produces a normal velocity at the wall, which is given by [49]:

$$\begin{cases} u_t = 0 \\ u_w = -\frac{D_v}{1-w_i}(\frac{\partial \omega}{\partial n})_i \end{cases} \tag{42}$$

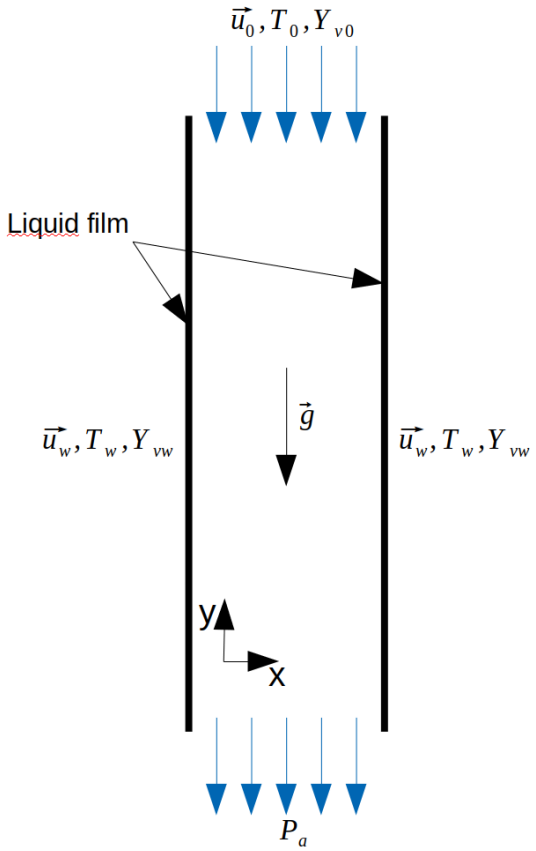

Figure 15: *Profiles of vertical velocity along a vertical line x=1800m at t=100s*

The inlet Reynolds number is 300 and the height and diameter of the channel are respectively 2m and 2cm. The mesh size is 0.5 mm, which gives a 40 x 4000 grid. The pressure p is assumed to be equal to the ambient pressure p_a for heights of the order of 1m. This leads to a constant value of $Y_{v,w}$, because the wall is also heated at a constant temperature T_w. Here, we chose to simulate a case from [16] with $T_w = T_0 = 327.5K$ and $Y_{v,w} = 0.1$. The kinematic viscosity ν is equal to $1.74e^{-5}m^2/s$ and the Schmidt number is equal to 0.529.

Results are presented on figures 16 and 17. The comparison is made between our results and those given in [16] on downwards velocity along the channel, at 0.2 m and at 1m.

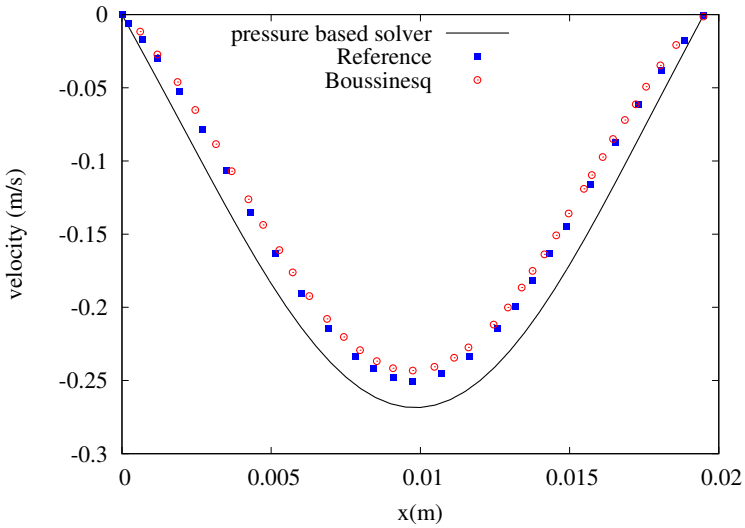

Figure 16: *Downwards velocity at 0.2m*

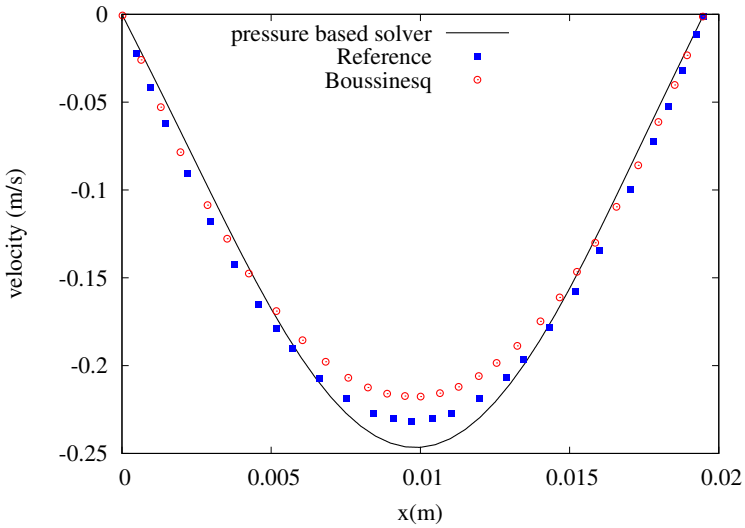

Figure 17: *Downwards velocity at 0.2m*

The results are in good agreement with the reference data, both in magnitude and tendency. Nevertheless, the discrepancies between the reference and our results is bigger than in the first test case. Several reasons can be invoked to explain these discrepancies: first, the boundary conditions are not applied in the same manner. In [16], source terms were introduced in the cells adjacent to the walls because direct implementation of special boundary conditions is not possible in the commercial software they use, which is a black box on this matter. Here, we directly impose the correct boundary conditions on the walls, without introducing the notion of adjacent cells. We prefer to use this second approach for the boundary conditions because it is identical to the original study [49], and also the article [50] on which the authors of the reference [16] rely. In fact, we assume that the liquid films are extremely thin so that boundary conditions for heat and mass transfer can be introduced as was suggested by Lin et al. [49]. Secondly,

they use a special formulation of the compressible flow equations: the density does not fully depend on the pressure, but only on the ambient pressure. In Ansys Fluent which is the commercial software that they are using, this special formulation is called the "Incompressible Ideal Gas Law", for which the density depends only on the operating pressure p_{op} and not on the local relative pressure field :

$$\rho = \frac{p_{op}}{R/WT} \tag{43}$$

This not the case in our solver because it is fully compressible, which means that the density fully depends on the local relative pressure and temperature. This could explain the discrepancies observed because we are not using the same formulation for the density. Indeed, the authors are already observing differences between their Boussinesq results and their Incompressible Ideal Gas Law results, so it seems logical that differences are also observed for our fully compressible model.

Regarding the density-based version of the Lattice Boltzmann Method, stability issues were encountered in this test case, which led to numerical instability before steady state was reached. According to [17], pressure-based solvers were initially designed to handle low-Mach flows with large density variations, which is typically the case here (multiphase interfacial flow). This comes from the fact that pressure-based solvers explicitly control pressure oscillations because the pressure is directly computed using an evolution equation instead of deducing it from an equation of state. In this case, we can assume that the density-based solver is unstable because it does not handle well the pressure oscillations caused by the large density variations at the walls, due to the presence of a thin liquid film. In order to stabilize the density-based simulations in this test case, we tried to refine the mesh in order to better capture and control the pressure oscillations at the walls. The mesh was refined 10 times, leading to a mesh composed of 16 million cells, leading to a dramatic growth of the computational cost, therefore demonstrating that the pressure-based method is more stable and robust and efficient on coarse meshes than the density-based method on this type of test cases. The coefficient σ in the HRR model [18] also had to be modified in order to stabilize the computation.

5 Conclusion

A new Lattice Boltzmann method for humid air able to fully account for compressibility effect was proposed and successfully assessed on several test cases. This method is an extension of the segregated pressure-based method proposed in [17] to the case of moist air with phase change. To this end, a modified equation of state is implemented, and the entropy equation used in the original scheme is replaced by an enthalpy equation, which is better suited to account for condensation and evaporation phenomena. New boundary conditions are also introduced in order to tackle the mass leakage issue at the boundaries, often encountered in large simulation domains. The present method is observed to be more accurate and more robust than the density-based Lattice Boltzmann method for humid air previously proposed in [14]. Indeed, the third test case about the heated vertical channel was only studied and validated with our compressible pressure-based model, because the compressible density-based code did not produce stable results and

the solution exploded. The pressure-based code is hence more general, since the density-based method was restricted to the Boussinesq approximation and weak dilatational effects. In fact, the compressible model is more accurate than the Boussinesq assumption but suffers from stability issues. These were handled thanks to the pressure-based code which is more stable than the density-based code, as shown in this paper thanks to the different test cases.

Acknowledgement

This work was performed using the ProLB software. Centre de Calcul Intensif d'Aix-Marseille is acknowledged for granting access to its high performance computing resources.

References

[1] G.J. Haltiner and F.L. Martin. *Dynamical and physical meteorology*. McGraw-Hill, 1957.

[2] M. Zerroukat and T. Allen. "A moist Boussinesq shallow water equations set for testing atmospheric models". In: *Journal of Computational Physics* 290 (2015), pp. 55–72. DOI: 10.1016/j.jcp.2015.02.011.

[3] D.D. Gray and A. Giorgini. "The validity of the boussinesq approximation for liquids and gases". In: *International Journal of Heat and Mass Transfer* 19.5 (1976), pp. 545–551. ISSN: 0017-9310. DOI: https://doi.org/10.1016/0017-9310(76)90168-X. URL: http://www.sciencedirect.com/science/article/pii/001793107690168X.

[4] S. Cherkasov, A. Anan'ev, and L. Moiseeva. "Limitations of the Boussinesq Model on the Example of Laminary Natural Convection of Gas between Vertical Isothermal Walls". In: *High Temperature* 56 (Nov. 2018), pp. 878–883. DOI: 10.1134/S0018151X18060081.

[5] M. Schatzmann and A.J. Policastro. "Effects of the Boussinesq Approximation on the Results of Strongly-Buoyant Plume Calculations". In: *Journal of Applied Meteorology and Climatology* 23.1 (1Jan. 1984), pp. 117–123. DOI: 10.1175/1520-0450(1984)023<0117:EOTBAO>2.0.CO;2. URL: https://journals.ametsoc.org/view/journals/apme/23/1/1520-0450_1984_023_0117_eotbao_2_0_co_2.xml.

[6] WP. O'Neill and R. Klein. "A moist pseudo-incompressible model". In: *Atmospheric research* 142 (2014), pp. 133–141.

[7] P.R. Bannon. "Theoretical foundations for models of moist convection". In: *Journals of the Atmospheric Sciences* 59.12 (2002), pp. 1967–1982. DOI: 10.1175/1520-0469(2002)059<1967:TFFMOM>2.0.CO;2.

[8] Y. Feng and W. Tao. "A Compressible Thermal Lattice Boltzmann Model with Factorization Symmetry". In: *Numerical Heat Transfer, Part B: Fundamentals* 66.6 (2014), pp. 544–562. DOI: 10.1080/10407790.2014.915679. URL: https://doi.org/10.1080/10407790.2014.915679.

[9] H. Luan et al. “Coupling of finite volume method and thermal lattice Boltzmann method and its application to natural convection”. In: *International Journal for Numerical Methods in Fluids* 70 (2011), pp. 200–221.

[10] F. Guiho, F. Alizard, and J.C. Robinet. “Global stability Analysis with Compressible CFD Solver”. In: June 2013. ISBN: 978-1-62410-214-1. DOI: 10.2514/6.2013-2620.

[11] W. Grabowski and P.K. Smolarkiewicz. “Monotone Finite-Difference Approximations to the Advection-Condensation Problem”. In: *Mon. Wea. Rev.* 118 (1990), pp. 2082–2097.

[12] P.K Smolarkiewicz, J. Szmelter, and F. Xiao. “Simulation of all-scale atmospheric dynamics on unstructured meshes”. In: *Journal of Computational Physics* 322 (2016), pp. 267–287. DOI: https://doi.org/10.1016/j.jcp.2016.06.048.

[13] J. W. Deardorff. “Usefulness of Liquid-Water Potential Temperature in a Shallow-Cloud Model”. In: *Journal of Applied Meteorology* 15.1 (1976), pp. 98–102. DOI: 10.1175/1520-0450(1976)015<0098:UOLWPT>2.0.CO;2.

[14] Y. Feng et al. “Hybrid recursive regularized lattice Boltzmann simulation of humid air with application to meteorological flows”. In: *Physical Review E* 100.2 (2019), p. 023304.

[15] G. Sommeria. “Three-Dimensional Simulation of Turbulent Processes in an Undisturbed Trade Wind Boundary Layer”. In: *Journal of the Atmospheric Sciences* 33.2 (Feb. 1976), pp. 216–241. ISSN: 0022-4928. DOI: 10.1175/1520-0469(1976)033<0216:TDSOTP>2.0.CO;2.

[16] N. Laaroussi, G. Lauriat, and G. Desrayaud. “Effects of variable density for film evaporation on laminar mixed convection in a vertical channel”. In: *International Journal of Heat and Mass Transfer* 52.1 (2009), pp. 151–164. DOI: https://doi.org/10.1016/j.ijheatmasstransfer.2008.05.022.

[17] G. Farag et al. “A pressure-based regularized lattice-Boltzmann method for the simulation of compressible flows”. In: *Physics of Fluids* 32 (June 2020), p. 066106. DOI: 10.1063/5.0011839.

[18] J. Jacob, O. Malaspinas, and P. Sagaut. “A new hybrid recursive regularised Bhatnagar–Gross–Krook collision model for Lattice Boltzmann method-based large eddy simulation”. In: *Journal of Turbulence* 19.11-12 (2018), pp. 1051–1076. DOI: 10.1080/14685248.2018.1540879.

[19] Christophe Coreixas et al. “Recursive regularization step for high-order lattice Boltzmann methods”. In: *Physical Review E* 96.3 (2017), p. 033306.

[20] A. Chorin. “A numerical method for solving incompressible viscous flow problems”. In: *Journal of Computational Physics* 2 (1967), pp. 12–26.

[21] S. Karni. “Hybrid Multifluid Algorithms”. In: *SIAM Journal on Scientific Computing* 17.5 (1996), pp. 1019–1039. DOI: 10.1137/S106482759528003X.

[22] R. Abgrall and S. Karni. “Computations of compressible fluids”. In: *Journal of Computational Physics* 169 (2001), pp. 594–623.

[23] O. Filippova and D. Haenel. “A novel lattice BGK approach for low Mach number combustion”. In: *Journal of Computational Physics* 129 (2001), pp. 267–274.

[24] O. Filippova and D. Haenel. "A novel numerical scheme for reactive flows at low Mach numbers". In: *Computer Physics Communications* 129.1 (2000), pp. 267–274. DOI: https://doi.org/10.1016/S0010-4655(00)00113-2.

[25] T. Lee and L. Ching-Long. "Pressure evolution lattice-Boltzmann-equation method for two-phase flow with phase change". In: *Phys. Rev. E* 67 (5 May 2003), p. 056703. DOI: 10.1103/PhysRevE.67.056703.

[26] P.R. Bannon. "Theoretical Foundations for Models of Moist Convection". In: *Journal of the Atmospheric Sciences* 59.12 (1Jun. 2002), pp. 1967–1982. DOI: 10.1175/1520-0469(2002)059<1967:TFFMOM>2.0.CO;2. URL: https://journals.ametsoc.org/view/journals/atsc/59/12/1520-0469_2002_059_1967_tffmom_2.0.co_2.xml.

[27] B. Maronga et al. "The Parallelized Large-Eddy Simulation Model (PALM) version 4.0 for atmospheric and oceanic flows: Model formulation, recent developments, and future perspectives". In: *Geoscientific Model Development* 8 (Aug. 2015), pp. 2515–2551. DOI: 10.5194/gmd-8-2515-2015.

[28] W.M. Washington and A. Kasahara. "A January simulation experiment with the two-layer version of the NCAR global circulation model". In: *Monthly Weather Review* 98.8 (Aug. 1970), pp. 559–580. DOI: 10.1175/1520-0493(1970)098<0559:AJSEWT>2.3.CO;2.

[29] T. Krüger et al. *The Lattice Boltzmann Method. Principles and Practice.* Springer, 2017.

[30] Z. Guo and C. Shu. *The Lattice Boltzmann Method and its applications in engineering.* World Scientific, 2013.

[31] A.A. Mohamad and A. Kuzmin. "A critical evaluation of force term in lattice boltzmann method, natural convection problem". In: *International Journal of Heat and Mass Transfer* 53 (2010), pp. 990–996.

[32] J. Jacob and P. Sagaut. "Wind comfort assessment by means of large eddy simulation with lattice Boltzmann method in full scale city area". In: *Build. Environ.* 139 (2018), pp. 110–124.

[33] L. Merlier, J. Jacob, and P. Sagaut. "Lattice-Boltzmann large-eddy simulation of pollutant dispersion in complex urban environment with dens gas effects: Model evaluation and flow analysis". In: *Building and Environment* 148 (2019), pp. 634–652.

[34] Y. Feng et al. "Hybrid recursive regularized thermal lattice Boltzmann model for high subsonic compressible flows". In: *Journal of Computational Physics* 394 (2019), pp. 82–99.

[35] S. Guo et al. "An efficient lattice Boltzmann method for compressible aerodynamics on D3Q19 lattice". In: *Journal of Computational Physics* 418 (2020), p. 109570.

[36] K.H. Kim, C. Kim, and O.H Rho. "Methods for the Accurate Computations of Hypersonic Flows: I. AUSMPW+Scheme". In: *Journal of Computational Physics* 174.1 (2001), pp. 38–80. DOI: https://doi.org/10.1006/jcph.2001.6873.

[37] C. Hirsch. *Numerical computation of internal and external flows: The fundamentals of computational fluid dynamics.* Elsevier, 2007.

[38] Y. Feng, P. Sagaut, and W. Tao. "A three dimensional lattice model for thermal compressible flow on standard lattices". In: *Journal of Computational Physics* 303 (2015), pp. 514–529. ISSN: 0021-9991. DOI: https://doi.org/10.1016/j.jcp.2015.09.011. URL: http://www.sciencedirect.com/science/article/pii/S0021999115005926.

[39] Y. Feng et al. "Regularized thermal lattice Boltzmann method for natural convection with large temperature differences". In: *International Journal of Heat and Mass Transfer* 125 (2018), pp. 1379–1391. DOI: 10.1016/j.ijheatmasstransfer.2018.05.051.

[40] M. Bouzidi, M. Firdaouss, and P. Lallemand. "Momentum transfer of a lattice fluid with boundaries". In: *Physics of Fluids* 13 (2001), pp. 3452–3459.

[41] B. Chun and A. J. C. Ladd. "Interpolated boundary condition for lattice Boltzmann simulations of flows in narrow gaps". In: *Phys. Rev. E* 75 (6 2007), p. 066705. DOI: 10.1103/PhysRevE.75.066705.

[42] J.C. Verschaeve and B. Muller. "A curved no-slip boundary condition for the lattice Boltzmann method". In: *Journal of Computational Physics* 229 (2010), pp. 6781–6803.

[43] I. Ginzburg and D. d'Humieres. "Local second-order boundary methods for lattice Boltzmann models". In: *Journal of Statistical Physics* 84 (1996), pp. 927–971. DOI: 10.1007/BF02174124.

[44] Y. Feng et al. "Solid wall and open boundary conditions in hybrid recursive regularized lattice Boltzmann method for compressible flows". In: *Physics of Fluids* 31 (2019), p. 126103.

[45] S. Wilhelm, J. Jacob, and P. Sagaut. "An explicit power-law-based wall model for lattice Boltzmann method-Reynolds-averaged numerical simulations of the flow around airfoils". In: *Phys. Fluids* 30 (2018), pp. 065111–1.

[46] S. Wilhelm, J. Jacob, and P. Sagaut. "A new explicit algebraic wall model for LES of turbulent flows under adverse pressure gradient". In: *Flow, Turbulence and Combustion* (2020), doi.org/10.1007/s10494-020-00181–7.

[47] N. Ouertatani et al. "Numerical simulation of two-dimensional Rayleigh–Bénard convection in an enclosure". In: *Comptes Rendus Mecanique* 336 (2008), pp. 12–26.

[48] W.W. Grabowski and T.L. Clark. "Cloud-environment interface instability: rising thermal calculations in two spatial dimensions". In: *Journal of Atmospheric Sciences* 48 (1991), pp. 527–546.

[49] T.F. Lin, C.J. Chang, and W.M. Yan. "Analysis of combined buoyancy effects of thermal and mass diffusion on laminar forced convection heat transfer in a vertical tube". In: *ASME Journal of Heat Transfer* 110 (1988), pp. 337–344.

[50] Y. Azizi et al. "Buoyancy effects on upward and downward laminar mixed convection heat and mass transfer in a vertical channel". In: *International Journal of Numerical Methods for Heat and Fluid Flow* 17.3 (2007), pp. 333–353. DOI: 10.1108/09615530710730193.